Thermoelectric Hotspot Cooling Using Thermally Conductive Fillers

Sang J. Park[a], Junyoung Park[a], Ki Mun Bang[a], Jung Min Lee[b], Woosung Park[b], Pawel Ziolkowski[c], and Hyungyu Jin[a,d]*

[a] *Department of Mechanical Engineering, Pohang University of Science and Technology (POSTECH), Pohang 37673, South Korea*
[b] *Department of Mechanical Systems Engineering, Sookmyung Women's University, Seoul 04310, South Korea*
[c] *German Aerospace Center (DLR) – Institute of Materials Research, Linder Hoehe, 51147 Cologne, Germany*
[d] *Institute for Convergence Research and Education in Advanced Technology, Yonsei University, Seoul 03722, South Korea*

* Corresponding author.

E-mail address: hgjin@postech.ac.kr (H. Jin).

Abstract

The commercial applications of thermoelectric coolers (TECs) are limited to niche markets owing to their low cooling efficiency. For hotspot cooling, in which the Fourier heat is added to the Peltier heat, thermoelectric (TE) materials should possess both large power factors and high thermal conductivities. However, the interdependence among TE material properties renders the development of such materials challenging. Herein, we provide a design strategy of TEC that addresses these material challenges at the device level. As proof of concept, we demonstrate that the cooling capability of filler-embedded TECs (F-TECs), which consist of TE legs with large power factors and a thermally conductive filler material, can be significantly improved compared to that of conventional TEC, owing to the 42.5% enhanced effective thermal conductance. Additionally, infrared imaging shows that the filler can decrease the temperature gradient and maximum temperature of the TE legs, which may improve the thermal stability of the TECs. Our proposed F-TEC concept can facilitate the development of effective TEC devices that can be widely used in hotspot cooling applications, such as in microprocessors, batteries and photovoltaic cells.

Nomenclature	
Bare	Conventional TEC without filler
BN0	Ecoflex–0wt.% BN composite or F-TEC using the composite as filler
BN23	Ecoflex–23wt.% BN composite or F-TEC using the composite as filler
BN33	Ecoflex–33wt.% BN composite or F-TEC using the composite as filler
COP	Coefficient of performance
c_p	Specific heat capacity (J/kg K)
e	Electron charge (C)
I_P	Electrical current intensity applied to the TECs or legs (A)
I_P^{Opt}	Optimal electrical current intensity for TEC operation (A)
L	Lorenz number (V^2/K^2)
K	Thermal conductance (W/K)
K_{Device}	Thermal conductance of the device including K_{TE} and K_{Filler} (W/K)
K_{Filler}	Thermal conductance of the filler (W/K)
K_{TE}	Thermal conductance of the TE legs (W/K)
k_B	Boltzmann constant (J/K)
m^*	Effective mass of the carrier (kg)
n	Carrier concentration (m^{-3})
PF	Power factor (= σS^2) ($W/(m{\cdot}K^2)$)
Q	Heat transfer rate (W)
Q''	Heat flux (W/m^2)
R_{TEC}	Electrical resistance of the TEC (Ω)
S	Seebeck coefficient (V/K)
TE	Thermoelectric
TEC	Thermoelectric cooler
F-TEC	Filler-embedded (high- K) TEC
T	Absolute temperature (K)
T_{Heat}	Absolute temperature at the head-loaded side of the TEC (K)
T_{Sink}	Absolute temperature at the heat sink of the TEC (K)

ΔT	Temperature difference at the ends of the TEC defined as $T_{\text{Heat}} - T_{\text{Sink}}$ (K)
ΔT_{Bare}	ΔT of the Bare sample
ΔT_{BN33}	ΔT of the BN33 sample
∇T	Temperature gradient (K/cm)
$T_{\text{Legs}}^{\text{Max}}$	Maximum temperature of the TE legs
zT	Thermoelectric figure of merit
Greek symbols	
α	Thermal diffusivity (mm^2/s)
η	Degree of improved cooling performance by the filler defined as $\Delta T_{\text{Bare}} - \Delta T_{\text{BN33}}$ (K)
μ	Carrier mobility (cm^2/V s)
κ	Thermal conductivity (W/m K)
κ_{ele}	Electron contribution on κ (W/m K)
κ_{eff}	Effective thermal conductivity defined as $\kappa_{\text{eff}} = \kappa + \frac{\text{PF} \cdot T_{\text{Heat}}^2}{2\Delta T}$ (W/m K)
κ_{Filler}	Thermal conductivity of the filler (W/m K)
κ_{lat}	Lattice contribution on κ (W/m K)
ρ	Mass density (kg/cm^3)
σ	Electrical conductivity (S/m)

1. Introduction

With the increasing miniaturization and densification of devices, the dissipation of localized heat has become a central issue in electronics, battery technologies, and photovoltaic cells [1–3]. According to various studies [4,5], a high heat flux exceeding 300 W/cm^2 can be generated at the hotspot of a microprocessor, which can cause a locally overheated region. To guarantee the performance and lifetime of devices that strongly depend on operating temperatures, these heat fluxes must be extracted instantly [3,6,7]. Although conventional convection-based cooling systems can dissipate such large heat fluxes, recent studies have pointed out that they can be inefficient in dissipating heat from small areas, in which handling zones are limited, owing to their bulky design and high thermal inertness [5,8,9]. In this regard, solid-state thermoelectric coolers (TECs) with various advantages can provide a suitable solution by applying the Peltier effect. These advantages include high-dynamic thermal transients (heat transfer rates), compact size, low weight, and the absence of mechanical moving parts and a working refrigerant; therefore, TECs are suitable for small-scale hotspot cooling [10–14]. However, despite the potential of TECs in heat-dissipation applications, their commercial use has been limited to niche markets because of their low cooling efficiencies [15].

The cooling efficiencies of TECs have been estimated using the coefficient of performance (COP), which generally depends on the thermoelectric (TE) figure of merit ($zT = \sigma S^2 T / \kappa$) of the constituent materials. Here, σ is the electrical conductivity, S is the Seebeck coefficient, κ is the thermal conductivity comprising the electronic (κ_{ele}) and lattice vibration (κ_{lat}) contributions, and T is the absolute temperature [16]. To improve the cooling efficiency, zT has been improved over the past decades by increasing the power factor (PF = σS^2) or decreasing the κ of TE materials [17]. A higher PF leads to an increase in the pumped heat by the Peltier effect owing to an increased S or a lowered internal power dissipation if the σ is increased. Lowering the κ improves the COP of refrigeration owing to the decreased Fourier heat flux. In refrigeration [17], the temperature of the heat-loaded side T_{Heat} is lower than that of the heat sink T_{Sink} (usually at room temperature) (**Fig. 1a**), and the direction of the active Peltier heat flow ($SI_{\mathrm{P}}T_{\mathrm{Heat}}$) owing to an applied current I_{P} through the TE legs is opposite to the direction of the passive Fourier heat flow ($K_{\mathrm{TE}}\Delta T$, where K_{TE} is the thermal conductance of the

TE legs and ΔT = T_{Heat} - T_{Sink}). As a low κ attenuates the backflow of Fourier heat that compensates for the Peltier heat, the use of zT by incorporating the denominator κ is justified as a criterion for determining the cooling efficiency. By contrast, in hotspot cooling [18,19], in which T_{Heat} is higher than T_{Sink}, the Peltier heat flows in the same direction as the Fourier heat (**Fig. 1b**). Here, a low κ decreases the Fourier heat transport by acting as a thermal barrier. Therefore, neither a high zT nor COP guarantees a high heat-dissipation capability in this case [18,19]. This distinctive feature of hotspot cooling necessitates specific material properties and an adapted device design. However, most commercial TECs have been optimized to achieve a high zT for refrigeration, which renders them a good thermal insulator (**Fig. 1c**). This optimization criterion has limited the widespread use of TECs for hotspot cooling conditions, which are found in most thermal management systems of electronics and batteries.

To address the aforementioned issue, Zebarjadi [18] highlighted the necessity of TE materials with a high κ and large PF, which are contrary to traditional high-zT materials. Adams *et al.* [19] and Li *et al.* [20] experimentally demonstrated TE hotspot cooling using high κ materials combined with large PFs such as $CePd_3$, Co, and Cu-Ni alloys. Additionally, as a criterion for designing efficient hotspot cooling materials, the effective thermal conductivity was suggested and expressed as follows [19]: $\kappa_{\mathrm{eff}} = \kappa + \frac{\mathrm{PF} \cdot T_{\mathrm{Heat}}^2}{2\Delta T}$, which includes the intrinsic thermal conductivity of the material and extrinsic PF-driven thermal conductivity. Nimmagadda and Sinha [21] used numerical simulations to study the TE properties required for transient on-chip cooling using a Si die. They determined that TE materials with a PF > 50 mW/m K^2 and κ > 100 W/m K are necessary to justify the use of TECs for on-chip hotspot cooling.

Despite the efforts to explore novel materials for hotspot cooling, the interdependence of S, σ, and κ complicates the simultaneous optimization of PF and κ of a material [22,23]. Specifically, S is inversely proportional to $n^{2/3}$ according to [22] $S = \frac{8\pi^2 k_B^2}{3eh^2} m^* T (\frac{\pi}{3n})^{2/3}$ for metals, which are promising material candidates for hotspot cooling, under the parabolic band and energy-independent scattering approximations. Here, n is the carrier concentration, m^* is the effective mass of the carrier, k_B is the Boltzmann constant, e is the electron charge, and h is the Planck constant. Additionally, σ is proportional to n according to $\sigma = ne\mu$, where μ is the carrier mobility. Furthermore, κ_{ele} is related to n by the Wiedemann–Franz law [16] $\kappa_{ele} = L\sigma T$ and thus is proportional to n, where L is the Lorenz number. Therefore, PF (σS^2) can be optimized at a specific n but κ_{ele} cannot [22], rendering the simultaneous optimization of PF and κ challenging.

As a way to circumvent such a material challenge, the efficiency of a TEC can also be improved by tailoring its structural design. In typical TECs for refrigeration, the gap between TE legs is filled with air or vacuum during operation, which allows most of heat flux to be conducted through the TE legs with low κ, making the overall device thermal conductance (K_{Device}) low. In contrast, for hot spot cooling, the gap between TE legs can be utilized as an additional thermal path to increase K_{Device}. For instance, the gap may be filled with an electrically-insulating and thermally-conducting filler material to provide an additional heat transfer channel (**Fig. 1d**). This strategy allows independent optimizations of K_{Device} and PF, since K_{Device} can be varied by filler design whereas PF can be optimized through TE material design.

In this study, we demonstrate a proof of concept of such a design strategy of TEC. For that, we fabricate a filler-embedded TEC (F-TEC) that consists of TE legs with high PFs and a high-κ filler material. We show that the cooling efficiency of such F-TECs is significantly improved compared to that of conventional TEC, owing to the enhanced K_{Device}. We systematically investigate the role of a filler on the cooling efficiency of a single type of a Peltier cooler module by varying its K_{Device} using various filler materials. Moreover, an infrared (IR) imaging is used to visualize the effect of the filler on the maximum temperature and temperature gradient in TE legs.

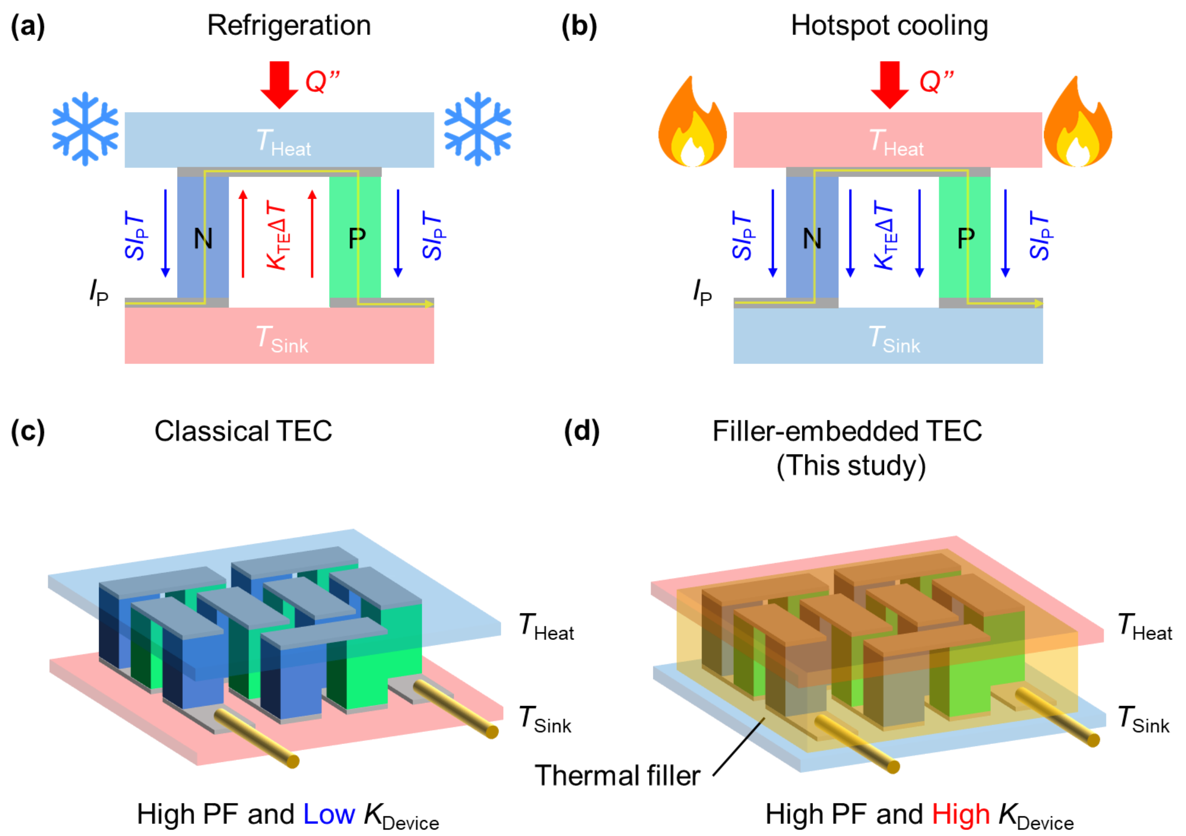

Fig. 1. Schematic of a thermoelectric cooler (TEC) used for (a) refrigeration and (b) hotspot cooling, in which the Peltier (SI_PT) and Fourier ($K_{TE}\Delta T$) heat flows have the opposite or same directions, respectively. Here, S, I_P, T, K_{TE}, and ΔT are the Seebeck coefficient, electrical current applied to the Peltier, absolute temperature, thermal conductance of thermoelectric legs, and temperature difference between heat loaded (T_{Heat}) and sink sides (T_{Sink}), respectively. Additionally, Q'' indicates the heat load required for heat dissipation. The effect of Joule heating is not shown for simplicity, each half of which is dissipated to the heat-loaded side and heat sink, respectively, for both cases. The corresponding optimized device structures with (c) low and (d) high device thermal conductance (K_{Device}) values. (d) Filler-embedded high K_{Device} TEC (F-TEC) proposed in this study.

2. Materials and methods

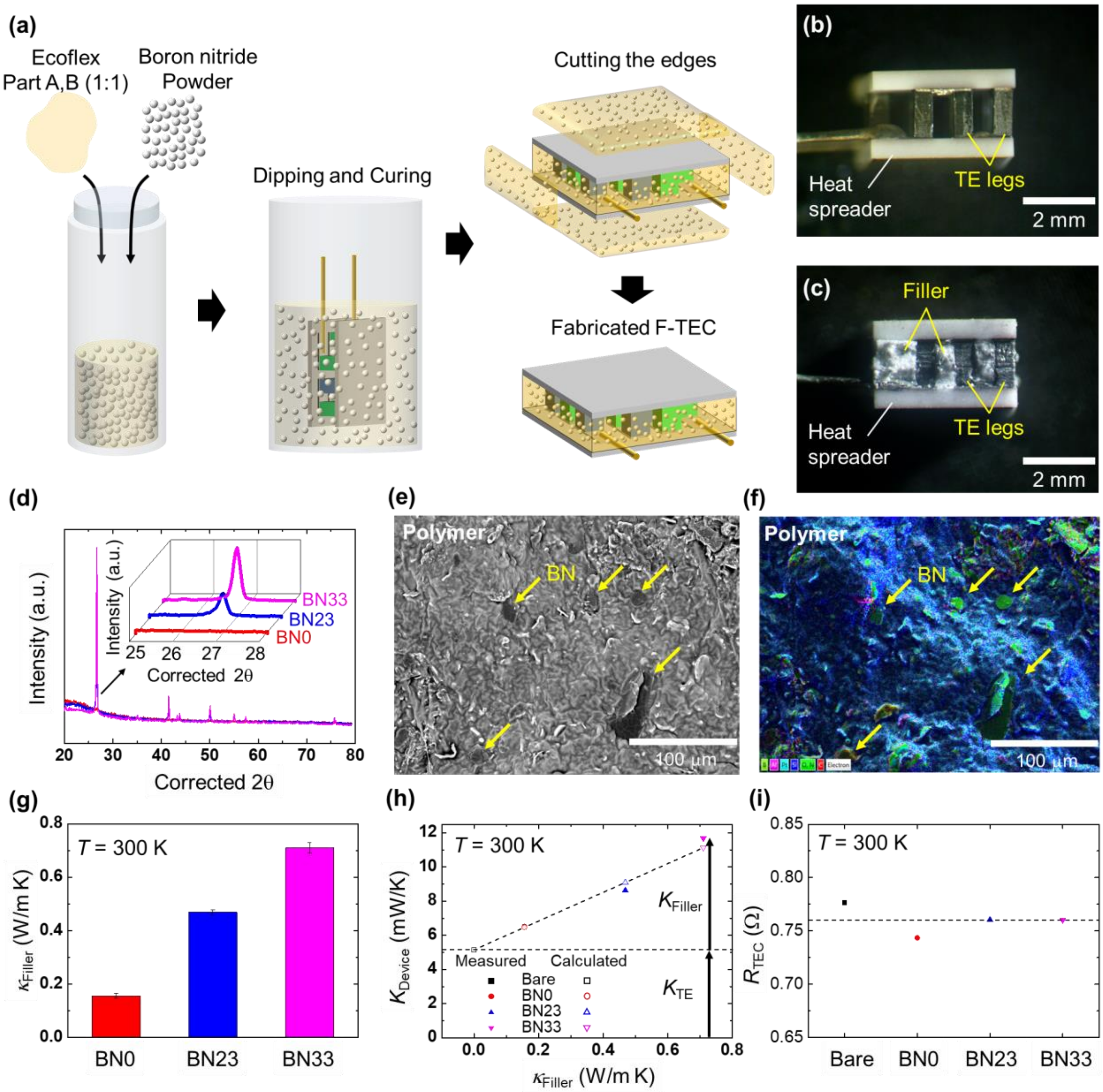

Fig. 2. (a) Fabrication process of filler-embedded thermoelectric coolers (F-TEC). Photographs of the (b) classical thermoelectric cooler (TEC) without a filler and (c) F-TEC. (d) X-ray diffraction patterns of the fillers. Additionally, 2θ is corrected using the Si [111] peak (not shown in the figure). The inset depicts the main peaks of BN. (e) Backscattered electron and (f) energy-dispersive X-ray spectroscopy images of the filler containing 33 wt.% BN powder. (g) Thermal conductivity of the fillers (κ_{Filler}). (h) Device thermal conductance (K_{Device}) measured and calculated based on the thermal conductance of the TE legs (K_{TE}) and

fillers (K_{Filler}) as a function of κ_{Filler} . The device conductance of the F-TEC was compared to the starting value without a filler, which is indicated by the horizontal dashed line. (i) Electrical resistance (R_{TEC}) of the TECs. All transport data were acquired at 300 K.

2.1 Fabrication of filler-embedded thermoelectric cooler (F-TEC)

The F-TECs used for hotspot cooling were fabricated by filling the interior of a TEC with a polymer–ceramic composite (**Fig. 2**). We selected polymer–ceramic composites as the filler materials in this study for the following reasons. First, the thermal conductivities of polymer–ceramic composites depend on the type and concentration of the ceramic additive material [24–27]; therefore, they provide an ideal platform to control the thermal conductance of a device (K_{Device}) by changing the composition as an experimental variable. In this study, we systematically investigated the impact of filler on K_{Device} and on the resulting cooling performance of the device, instead of simply maximizing the K_{Device}. Second, polymers do not cause significant thermal stress in the TECs during fabrication and cooling operations because of their elasticity and softness. Finally, polymers and ceramics are generally electrically insulating, which prevents electrical interference, such as shunting and electromagnetic heating, with the operation of TE legs. Commercially available polymer Ecoflex (Ecoflex 00-30, Smooth-on) and agglomerated BN powder (CFA 250S, 3M Co., Ltd.) were used as the constituents of the composite. Since the viscosity of a polymer–ceramic mixture rapidly increases with increasing the mass fraction of the ceramic component [28,29], a polymer formulation with low viscosity is preferred in fillers. Ecoflex 00-30 was chosen because it possesses low viscosity [30] and thus its composite mixtures are suitable for filling the complex inside the TECs (**Figs. 1 and 2b**). BN is an electrically insulating and thermally conductive material that is lightweight with a large energy band gap. Furthermore, BN is robust to oxidation and chemical reactions and exhibits high thermal stability [25,26]. The BN power used in this study was agglomerated and consequently thermally isotropic [31].

The Ecoflex–BN composite samples were prepared by mixing the base and curing agents of Ecoflex in a 1:1 weight ratio (wt.%) (**Fig. 2a**). After vacuuming the Ecoflex mixture to remove pores, BN powders were added to the Ecoflex mixture in the mass fractions of 23 and 33 wt.% of the total mass, which includes both BN and polymer. Generally, a high ceramic concentration imparts a high thermal conductivity to the resulting composite. In this study, 33 wt.% of BN was the maximum mass fraction of BN since higher concentrations become too viscous to firmly fill the complex inside the millimeter-sized TEC (**Fig. 2b**). Subsequently, commercial TECs (NL1010T-01AC, Marlow Industries Inc.) with a high PF and low K_{Device} were dipped into the different Ecoflex–BN mixtures and vacuumed. The detailed structure of the TEC can be found in **Fig. S1** in **Supplementary Information**. The F-TEC samples were cured at 393 K for 2 h and finally shaped into their original dimensions by cutting off the protruding parts of the solidified fillers (**Figs. 2a and c**). Four samples were used for this study, i.e., one reference TEC without a filler and three experimental F-TECs, which were prepared with Ecoflex fillers containing 0, 23, and 33 wt.% BN powder. These samples are labeled Bare, BN0, BN23, and BN33, respectively, according to the mass fraction of BN in the filler (**Table 1**).

Table 1. Thermal properties of the samples at 300 K (blanks: irrelevant properties).

Sample label	**BN concentration of the filler [wt.%]**	**Thermal conductivity of the filler κ_{Filler} [W/m K]**	**Thermal conductance of the device K_{Device} [mW/K]**
Bare	-	-	5.15
BN0	0	0.156	6.52
BN23	23	0.469	8.63
BN33	33	0.710	11.67

2.2 Structural analysis of filler

The crystal structures of the Ecoflex–BN composite fillers were investigated by measuring the X-ray diffraction (XRD) patterns using a combination of Cu-Ka1 and Ka2 radiation with an average wavelength of λ = 1.5418 Å (D2 phaser, Bruker). The polymer-based samples may cause a significant misalignment in the XRD measurements owing to sample warping and elasticity; therefore, the fillers were carefully molded to maintain a flat surface, and crystalline Si powder was sprinkled onto the samples to correct the misalignment-induced 2θ shift (See ref. [32] for the technical details). In addition, the 2θ, based on wavelength λ = 1.5418 Å, was converted to the commonly used 2θ based on Cu-Ka1 with λ = 1.5406 Å. The microstructures of the Ecoflex–BN composites were investigated using the back-scattered electron mode in field emission scanning electron microscopy (JSM-IT800HL, JEOL) combined with energy-dispersive X-ray spectroscopy (EDS).

2.3 Thermal and electrical properties of filler and F-TEC

The thermal conductivity of each filler κ_{Filler} was obtained by multiplying the thermal diffusivity α, mass density ρ, and specific heat c_{P} as follows: $\kappa_{\mathrm{Filler}} = \alpha \times \rho \times c_{\mathrm{p}}$ [33]. The Ecoflex–BN composites were carefully molded into 12.7 mm diameter disks for measuring α. The samples were coated with a graphite spray (Graphit-33, Kontakt Chemie), and α was measured by laser flash analysis (LFA 467, Netzsch), during which the temperature was increased from 300 to 400 K in 20 K increments. This corresponded to the temperature range required for the active cooling experiment described in **Section 3** (**Fig. 3**). The densities of the composites were obtained using Archimedes' method (XS105, Mettler Toledo) at room temperature (295 K), and the specific heat was measured using differential scanning calorimetry (Q200, TA instruments) while increasing the temperature from 300 to 400 K at a heating rate of 5 K/min.

The K_{Device} values of the F-TECs were evaluated via the steady-state method [33] using a customized liquid nitrogen cryostat system (Lake Shore Cryotronics, Inc.) according to $Q = K_{\mathrm{Device}}\Delta T$ with Q being the heat flow rate and ΔT the temperature difference across the sample (**Fig. 3a**). Two T-type thermocouples for measuring $\Delta T = T_{\mathrm{Heat}} - T_{\mathrm{Sink}}$ were attached to the heat spreaders at the heat-loaded side (T_{Heat}) and at the heat sink (T_{Sink}) using silver epoxy (H20E, EPO-TEK). Here, Cu and constantan wires with a diameter of 25.4 μm (SPCP- and SPCI-001-50, Omega Engineering, Inc.) were used to form thin thermocouples to minimize heat losses along the wires. Subsequently, a 1000 Ω resistive heater (SGD-7/1000-LY13, Omega Engineering, Inc.) was connected using wires with a diameter of 76.2 μm. The heat flow rate

Q was determined according to $Q = I_H V_H$ with I_H being the supplied electric current to the heater and V_H the corresponding voltage drop measured by a multimeter (2000, Keithley). The heater was attached to a BeO heat spreader with high thermal conductivity (κ ~ 300 W/(m K) [34]) and subsequently placed on the top of TEC with thermal grease in between (H grease, Apiezon) to improve the thermal contact resistance and to homogenize the temperature distribution and heat flux at the hot side of the TEC. The thermocouple voltages for measuring T_{Heat} and T_{Sink} were monitored using a nanovoltmeter (2182A, Keithley) while applying I_H = 3 mA to the heater using a current source (6221, Keithley). The T_{Sink} was maintained at 300 K during the measurement. All measurements were conducted in the cryostat under a high vacuum of ~ 10^{-4} Pa and under the cover of a gold-plated radiation shield to minimize heat losses by convection and radiation, respectively. These heat losses were consequently not considered for the determination of K_{Device}.

3. Experimental results and discussion

3.1 Structural analysis of filler

First, the crystal structure of the fillers was investigated to verify that the thermally conductive BN was well embedded into the polymer as a form of composite. The XRD patterns in **Fig. 2d** revealed a clear BN peak, which increased with increasing the mass fraction of BN, while BN0 (Ecoflex) exhibited a broad peak that indicated an amorphous structure of the polymer. The backscattered electron image in **Fig. 2e** shows that the lighter elements B and N appear to be dark compared with the bright area of Ecoflex matrix with the heavier element Si. The composition of the dark dots was verified to be B and N using the corresponding EDS maps (**Fig. 2f**). These results indicated the absence of a chemical reaction between BN and Ecoflex for the fabrication process.

3.2 Controlling the thermal properties of filler and F-TEC

Next, we investigated the effect of the concentration of embedded BN on the thermal properties of the Ecoflex–BN composites. **Figure 2g** shows that κ_{Filler} at 300 K is 0.156, 0.469, and 0.710 W/m K for BN0, BN23, and BN33, respectively. The maximum concentration of BN33 provides an overall increase of thermal conductivity of 355% compared to pure Ecoflex (BN0). The results are summarized in **Table 1**, while details including the thermal diffusivity α, density ρ, specific heat c_p, and temperature dependence of κ_{Filler} can be found in **Fig. S2** in **Supplementary Information**.

Then, we quantified the effect of the composite fillers on K_{Device}. As shown in **Fig. 2h**, K_{Device} monotonically increases with increasing thermal conductivity of the filler κ_{Filler}. BN33 exhibited the highest K_{Device} of 11.67 mW/K at 300 K, which was 127% higher than that of Bare (K_{TE} = 5.15 mW/K). The measured K_{Device} was in good agreement with its calculated counterpart, which was determined under the assumption of a parallel thermal connection[33] between the TE legs and the filler (i.e., $K_{Device} = K_{TE} + K_{Filler}$). K_{TE} was kept constant for all calculations, while K_{Filler} was estimated using κ_{Filler} and the TE fill factor (~24%), which is the fractional area coverage of the TE legs per unit substrate area [35]. Furthermore, evaluating results for the sample Bare (without filler) at 300 K with $K_{Device} = K_{TE}$ = 5.15 mW/K revealed a thermal conductivity κ_{TE}= 1.91 W/m K for the TE legs, which is in good accordance with typical values reported for Bi-Te-based TE materials [36–38]. The deviation between the measured and calculated values may be attributed to uncontrolled pores in the filler in the TEC or the thermal contact resistance between the filler and TEC, which were neglected for the K_{Device} calculation. The temperature-dependent K_{Device} data are presented in **Fig. S3** for the range 300–400 K.

Although thermocouples and heater wires attached for K_{Device} measurement (See **Section 2** for details) have small diameters of 25.4 and 76.2 μm, respectively, heat loss through the wires was inevitable and resulted in an overestimation of the applied Q'' and K_{Device}. It is noted that the total thermal conductance of the attached wires lies in the range 0.140–0.186 mW/K, which equals a few percentages of K_{Device} whose maximum value is 3.6% for Bare. The standard uncertainty of thermocouple voltage measurements is typically less than 0.2% and has a maximum of 0.38%, estimated from the standard deviation of twenty-five repeated measurements.

To verify whether the thermoelectric properties of the TE legs are affected by the embedding of the fillers, we measured the electrical resistance R_{TEC} of the samples using the four-probe [39] and Delta mode measurements [40] (6221/2182A, Keithley) at 300 K in the cryostat. The standard measurement uncertainty was determined to be less than 0.001%. **Figure 2g** displays the R_{TEC} values of the TEC and F-TEC samples, which are in the range 744–777 mΩ with a standard deviation of 11.7 mΩ. As the R_{TEC} values of three different Bare samples were in the range 761–791 mΩ with a similar standard deviation of 12.4 mΩ (**Fig. S4**), we consider that the deviation of the R_{TEC} values for F-TEC samples was neither caused nor influenced by the degradation of the TE legs during fabrication and measurement but just a result of typical manufacturing tolerances. These results indicated that the thermal conductance of the device can be separately optimized at the device level without significantly affecting the thermoelectric properties by embedding the interior of the TEC with thermal fillers. In the following sections, we discuss the improvement in the cooling performances of the F-TECs owing to the K_{Device} enhanced by the fillers.

3.3 Evaluation of the heat-dissipation capabilities of the F-TECs

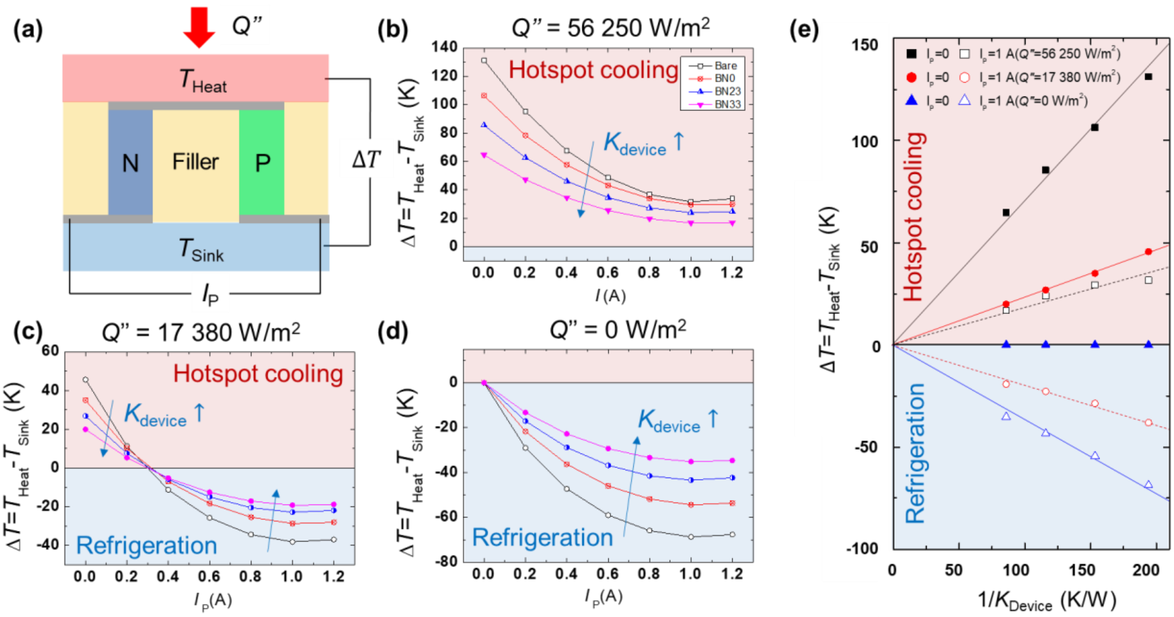

Fig. 3. (a) Experimental configuration for evaluating cooling performance. Temperature difference between the heat-loaded side and the heat sink under the heat flux Q'' of (b) 56

250, (c) 17 380, and (d) 0 W/m^2. (e) Temperature difference as a function of device thermal resistance ($1/K_{\mathrm{Device}}$). All data were acquired at T_{Sink} = 300 K.

The cooling performance of the F-TECs was evaluated by monitoring the temperature difference ΔT between the heat-loaded T_{Heat} and sink T_{Sink} sides ($\Delta T = T_{\mathrm{Heat}} - T_{\mathrm{Sink}}$) at T_{Sink} = 300 K (**Fig. 3**). ΔT was measured using the thermocouples in the cryostat (**Section 2**). The measurements have been conducted under various heat fluxes that corresponded to different operation modes such as hotspot cooling (Q'' = 56 250 W/m^2 in **Fig. 3b**), refrigeration (Q'' = 0 W/m^2 in **Fig. 3d**), and at intermediate conditions (Q'' = 17 380 W/m^2 in **Fig. 3c**) (Refer to **Fig. 1** and **Introduction** for details). An electrical current I_{P} was applied to the TECs by a current source (E3546A, Agilent) in the range 0–1.2 A in 0.2 A increments. The TECs exhibited the best performance at I_{P} = 1 A; a further increase in I_{P} caused the cooling performance to degrade owing to Joule heating.

First, we discuss the cooling performance at Q'' = 56 250 W/m^2 that corresponds to the hotspot cooling situation for all I_{P} values. As shown in **Fig. 3b**, ΔT decreases in F-TECs compared to the classical TEC owing to the increased Fourier heat conduction due to the filler. When no current was applied (I_{P} = 0 A), at which the Peltier effect was absent and Fourier conduction dominated (**Fig. S5**), ΔT decreased from 131.24 K for Bare (ΔT_{Bare}) to 64.616 K for BN33 (ΔT_{BN33}). When I_{P} = 1 A was applied, at which the Peltier effect delivered the highest cooling performance and dominated (**Fig. S5**), ΔT decreased from ΔT_{Bare} = 31.599 K to ΔT_{BN33} = 16.764 K. The degree of improved cooling performance by the filler, defined as $\eta = \Delta T_{\mathrm{Bare}} - \Delta T_{\mathrm{BN33}}$, decreased while the increase in I_{P} decreased the contribution of Fourier conduction compared to that of the Peltier effect (Refer to **Fig. S5** for the quantitative analysis). In this case, the filler-induced high K_{Device} improved the cooling performance by providing an additional heat path that contributed to Fourier conduction. Next, we investigated the cooling performance under Q'' = 0 W/m^2 that corresponded to refrigeration, in which the direction of the Fourier heat flow was opposite to that of the Peltier heat flow. In contrast to hotspot cooling, $|\Delta T_{\mathrm{BN33}}|$ was smaller than $|\Delta T_{\mathrm{Bare}}|$ for all I_{P} values. In this case, the filler-induced high K_{Device} degraded the cooling performance by increasing Fourier conduction, which compensated for the Peltier effect. Lastly, we demonstrated the case of Q'' = 17 380 W/m^2, wherein both hotspot cooling and refrigeration modes occur depending on the value of I_{P} (**Fig. 3c**). At low I_{P}, hotspot cooling is at work, while refrigeration occurs at high I_P. The F-TECs performed better than the Bare sample in hotspot cooling (where $I_P < \sim 0.3$ A), whereas the performances of the F-TECs were worse than that of the Bare sample in refrigeration (where $I_P > \sim 0.3$ A). This coincided with the results obtained from the previous cases. To further clarify that the improved and degraded cooling performances for the hotspot cooling and refrigeration situations, respectively, originated from the filler-induced K_{Device} engineering, we plotted ΔT at $I_P = 0$ and 1 A as a function of the device thermal resistance $1/K_{Device}$ **(Fig. 3e)**. The fitted lines in **Fig. 3e** indicate that ΔT increases linearly with the increase in $1/K_{Device}$ for hotspot cooling and refrigeration. The minimum coefficient of determination (adjusted R^2) of the fitted curves was 0.99713 for $I_P = 0$ A and 0.98739 $I_P = 1$ A, which implied that the increased K_{Device} directly improved and degraded the cooling performances of the TECs in hotspot cooling and refrigeration situations, respectively, without substantially affecting the thermoelectric properties of the TE legs. The deviation in ΔT from the fitted lines, which was especially relatively large for $I_P = 1$ A, possibly occurred from the slight differences in R_{TEC} values (**Fig. 2i**).

We anticipate that the increased thermal conductance in F-TECs demonstrated in this study could offer broader applications beyond the low heat flux range of $\sim 10^4$ W/m^2 studied here. Specifically, this approach may be applicable to high heat flux ranges of $\sim 10^6$ W/m^2 relevant for electronic device cooling [4,5]. To further explore this potential, we calculated the cooling performance of (F-)TEC under the heat flux of $Q'' = 3\times10^6$ W/cm^2 as a function of device thickness, as shown in **Fig. S6** in the Supplementary Information. As the device thickness decreases to ~ 50 μm, a typical thickness of TE tin films that can be fabricated using various deposition techniques [5,13], the F-TEC with high K_{Device} still exhibits superior performance with $T_{Heat} = 329$ K compared to TEC without filler ($T_{Heat} = 350$ K). Overall, our findings suggest promising opportunities for improving the performance of TE devices for a range of applications, including high heat flux electronic device cooling.

Even though most applications that require substantial heat dissipation are hotspot cooling situations [5,41], in which the proposed F-TECs can be advantageous, one may expect to develop a universal F-TEC that can be applied to all cooling situations, including hotspot cooling, refrigeration, and their intermediate. To achieve this, we may introduce a filler that has a large K_{Filler} for $T_{Heat} > T_{Sink}$ (for hotspot cooling) and a small K_{Filler} for $T_{Heat} < T_{Sink}$ (for refrigeration). In particular, thermal diode materials and structures [42–44] can be suitable fillers as their thermal conductivities can be modulated using a magnetic field [32,45], electric field [46,47], and thermal energy [48].

3.4 COP and effective thermal conductance of the F-TECs in hotspot cooling

The COP, defined as the heat dissipation from the heat-loaded side Q_{Heat} per input electrical power P_{Sup}, has been used to evaluate the cooling efficiency of TECs

$$\text{COP}=\frac{Q_{\text{Heat}}}{P_{\text{Sup}}} \tag{1}$$

The heat dissipation from the heat-loaded side can be determined by a net energy balance (**Fig. 1a and 1b**):

$$Q_{\text{Heat}} = S_{\text{TEC}} T_{\text{Heat}} I_{\text{P}} + K_{\text{Device}} (T_{\text{Heat}} - T_{\text{Sink}}) - \frac{1}{2} I_{\text{P}}{}^{2} R_{\text{TEC}} \tag{2}$$

From the first law of thermodynamics, input electrical power can be defined as $P_{\text{Sup}} = Q_{\text{Heat}} - Q_{\text{Sink}}$ the difference between the heat dissipations from the heat-loaded side and to the heat sink Q_{Sink}, and expressed as

$$P_{\text{Sup}} = I_{\text{P}}{}^{2} R_{\text{TEC}} - S_{\text{TEC}} I_{\text{P}} (T_{\text{Heat}} - T_{\text{Sink}}) \tag{3}$$

Combining **Eqs. (1)–(3)**, the COP can be expressed as

$$\text{COP} = \frac{S_{\text{TEC}} T_{\text{Heat}} I_{\text{P}} + K_{\text{Device}} (T_{\text{Heat}} - T_{\text{sink}}) - \frac{1}{2} I_{\text{P}}{}^{2} R_{\text{TEC}}}{I_{\text{P}}{}^{2} R_{\text{TEC}} - S_{\text{TEC}} I_{\text{P}} (T_{\text{Heat}} - T_{\text{sink}})} \tag{4}$$

As mentioned in the **Introduction**, the COP is a good indicator to evaluate the cooling efficiency in refrigeration. However, in hotspot cooling, the COP cannot be applied as in the refrigeration case, since the portion of Fourier heat flux $K_{\text{Device}}(T_{\text{Heat}} - T_{\text{Sink}})$ leads to an infinite COP at $I_{\text{P}} = S(T_{\text{Heat}} - T_{\text{Sink}}) / R_{\text{TEC}}$, according to **Eq. (4)**. For a detailed discussion on the limitations of using COP in a hotspot cooling scenario, refer to the Section S7 of the Supplementary Information. Accordingly, we present the cooling efficiency of the TECs in hotspot cooling by means of effective thermal conductance $K_{\mathrm{TEC}}^{\mathrm{Eff}}$, proposed by Adams *et al.* [19]. The $K_{\mathrm{TEC}}^{\mathrm{Eff}}$ captures the maximum heat dissipation of TECs $Q_{\mathrm{Heat}}^{\mathrm{Max}}$ at an optimal current $I_{\mathrm{P}}^{\mathrm{Opt}}$. By taking the derivative of **Eq. (2)**, the optimal current and maximum heat dissipation can be determined as

$$I_{\mathrm{P}}^{\mathrm{Opt}} = S_{\mathrm{TEC}} T_{\mathrm{Heat}} / R_{\mathrm{TEC}} \tag{5}$$

$$Q_{\mathrm{Heat}}^{\mathrm{Max}} = (K_{\mathrm{Device}} + \frac{(S_{\mathrm{TEC}} T_{\mathrm{Heat}})^2}{2 R_{\mathrm{TEC}} \Delta T}) \Delta T \tag{6}$$

Analogous to Fourier's law $Q = K\Delta T$, the effective thermal conductance of TEC is defined in **Eq. (6)** as follows [19]

$$K_{\mathrm{TEC}}^{\mathrm{Eff}} = K_{\mathrm{Device}} + \frac{(S_{\mathrm{TEC}} T_{\mathrm{Heat}})^2}{2 R_{\mathrm{TEC}} \Delta T} \tag{7}$$

, which includes the passive thermal conductance by the Fourier conduction (K_{Device}) and active thermal conductance by the Peltier effect ($\frac{(S_{\mathrm{TEC}} T_{\mathrm{Heat}})^2}{2 R_{\mathrm{TEC}} \Delta T}$). By applying experimentally quantified parameter values, $K_{\mathrm{TEC}}^{\mathrm{Eff}}$ of the (F-)TEC samples were determined and compared at ΔT = 100 K (**Fig. 4**). $K_{\mathrm{TEC}}^{\mathrm{Eff}}$ monotonically increases as K_{Device} increases owing to the additional contribution of the filler. Accordingly, the BN33 sample exhibits a 42.5% larger $K_{\mathrm{TEC}}^{\mathrm{Eff}}$ (21.86 mW/K) compared to the Bare sample ($K_{\mathrm{TEC}}^{\mathrm{Eff}}$ = 15.34 mW/K), which corresponds to the previous observation in hotspot cooling (**Fig. 3b**).

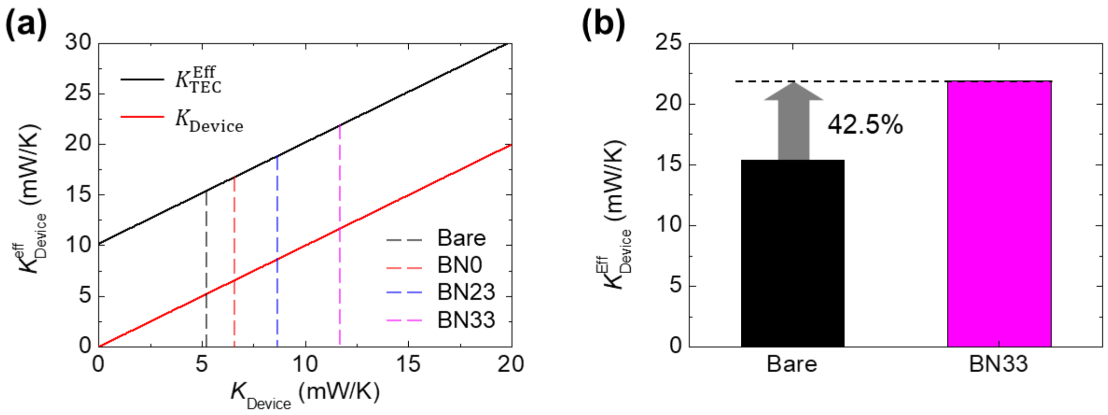

Fig. 4. (a) Effective thermal conductance of the samples K_{TEC}^{Eff} calculated based on T_{Heat} = 400 K and T_{Sink} = 300 K and passive thermal conductance K_{Device}. The vertical dashes lines correspond to K_{Device} of the experimental samples. (b) Comparison of K_{TEC}^{Eff} between Bare and BN33.

3.5 Visualization of the temperature gradient using an IR camera

Considering the TE fill factor of ~ 0.24 of the Bare sample, the TE legs experienced a large heat flux exceeding 234 000 W/m^2 and longitudinal temperature gradient ∇T exceeding 65.6 K/mm under the heat load condition Q'' = 56 250 W/m^2 (**Section 3.3**). Such large ∇T applied to the TE legs may affect to the thermal stability of the TE legs and the lifespan of the TECs. We visualized the temperature profile of the TE legs under hotspot cooling using an IR camera (Image IR 7300, InfraTec). The technical details of IR imaging can be found in the authors' previous papers [49,50]. In TECs, the ∇T is forming from individual contributions of (1) a linear temperature profile due to Fourier heat conduction and Peltier heat flow, and (2) a parabolic temperature profile due to current-induced volumetric Joule heating [19,33]. To investigate the ∇T generated by both effects, the temperature profile of TE legs was recorded by applying Q'' = 46 500 W/m^2 to the heat-loaded side of TECs, and I_P = 0 and 1 A to the TECs (**Fig. 5**). The Q'' of 46 500 W/m^2 was the maximum value that could be applied for the IR experiment. Although it is smaller than that in the cooling performance evaluation, it still corresponds to the hotspot cooling case. Note that the Peltier, Fourier, and Joule heating effects determined the longitudinal temperature profile, even though the TEC lost heat by natural air convection during the IR experiment.

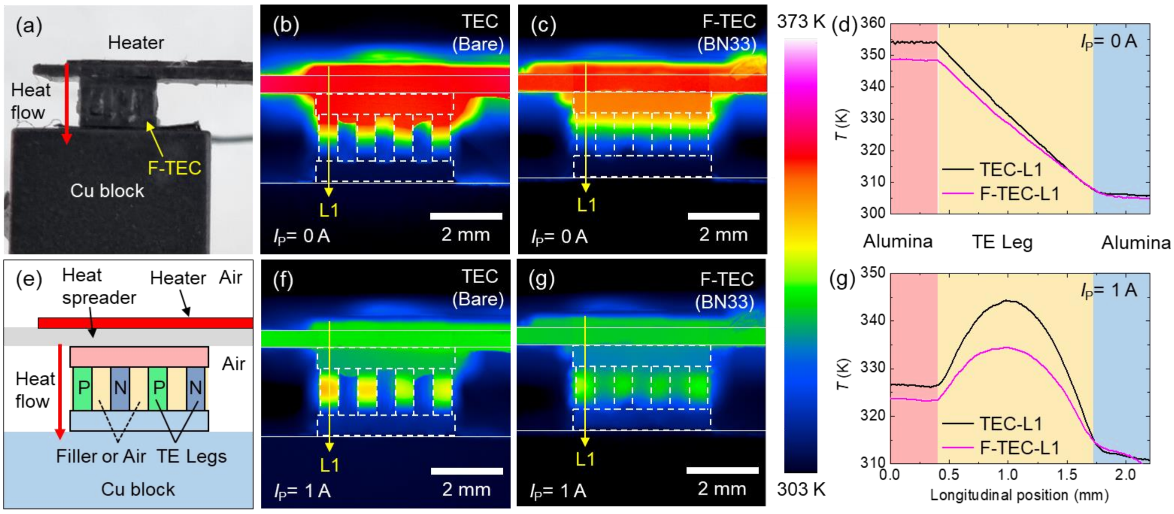

Fig. 5. (a) Photograph and (e) Schematic illustration of experimental configurations for IR visualization. A heat flux of 46 500 W/m^2 was applied by the heater. Temperature contour of TEC (Bare) for (b) $I_P = 0$ A and (f) $I_P = 1$A. Temperature contour of F-TEC (BN33) for (c) $I_P =$ 0 A and (g) $I_P = 1$A. The white lines are guides to the eye, indicating the boundaries of TE legs, filler, heat spreaders, and Cu block. Temperature profiles of the TEC and F-TEC for (d) $I_P = 0$ A and (g) $I_P = 1$ A following the line (L1) through a TE leg sandwiched between alumina heat spreaders.

The IR tests were conducted with the TEC (Bare) and F-TEC (BN33) samples, which were covered by a graphite spray for the uniform emissivity of their side faces (**Fig. 5a**). The IR signals of each pixel were recorded and subsequently converted to the corresponding temperatures using pre-calibrated data. For $I_P = 0$ A, only Fourier heat flowed through the configurations yielding almost uniform ∇T along the TE legs of the TEC and F-TEC (**Figs. 5b** and **c**). The corresponding temperature profiles along the longitudinal line (L1) from the heat-loaded side to the heat sink were almost linear in the TE legs (**Fig. 5d**), indicating that the longitudinal heat load and not air convection dominated the longitudinal temperature profile. The TE leg in the F-TEC exhibited a smaller temperature profile and ∇T than those in the TEC owing to the heat dissipation by filler. As a result, the heat-loaded side in F-TEC exhibited lower temperature (T_{Heat} ~ 348 K) compared to TEC (T_{Heat} ~ 354 K), although the F-TEC experienced a larger heat load than the TEC because of larger thermal conductance. Based on simple calculation for the heat losses by air convection with natural heat transfer coefficient of 5–20 W/m^2 K [33], the F-TEC experienced 12–39% higher heat load than the TEC from the heater, which led to a conservative estimation of ∇T inside the F-TEC compared to the TEC. Next, I_P = 1 A was applied to both TECs with the same experimental conditions. The generated heat inside the TE legs by Joule heating is equal for the TEC and F-TEC unless different module properties exist. The Joule heat is partially dissipated from the legs to the gaps in between. In the case of the F-TEC, this dissipation is much higher owing to the higher thermal conductivity of the filler compared to air in TEC. Therefore, the TE legs in BN33 exhibited a smaller ∇T and maximum temperature of the legs ($T_{\text{Legs}}^{\text{Max}}$ = 334.4 K) in comparison with those of Bare ($T_{\text{Legs}}^{\text{Max}}$ = 344.3 K) (**Fig. 5g**). The temperature profiles in **Fig. 5g** confirm the parabolic temperature profile due to Joule heating with a maximum at the middle of the legs. The slight difference in temperature distribution between the TE legs (**Figs. 5f and g**) possibly resulted from the differences in (1) TE properties of n- and p-type materials such as σ, S, and κ or (2) the heat transfer condition at the surfaces facing to air or filler. These results clearly implied that the embedded filler in the F-TECs reduced the ∇T along the TE legs.

4. Conclusion

We proposed a novel TEC device concept for hotspot cooling applications by embedding the interior of a commercial TEC with a thermally conductive and electrically insulating filler material. The filler improves the integral thermal device conductance K_{Device} of the F-TEC, which is an important parameter for hotspot cooling, by opening a new heat conduction path next to the conduction through the TE legs. In this way, the proposed F-TEC can overcome the engineering challenges at the material level that are caused by the interdependence among the TE parameters, which impedes the individual adjustment of thermal and thermoelectric transport properties. Consequently, the relatively easy application of a thermally conductive filler material provides an additional degree of freedom to the system design. Embedding a filler into a TEC enables the independent control of Fourier heat conduction without any influence on the Peltier-driven heat transport. The F-TECs were experimentally demonstrated using various Ecoflex–BN composite fillers, with which K_{Device} was systematically controlled at 300 K in the range of 5.15–11.67 mW/K (127% change). The cooling performances of the F-TECs improved owing to the fillers; the hotspot temperature under the heat flux Q"= 56 250 W/m^2 decreased from 431.2 K (Bare) to 364.6 K (BN33) at I_{P} = 0 and 331.6 K to 316.8 K at I_{P} = 1 A. The effective thermal conductance ($K_{\mathrm{Device}}^{\mathrm{eff}}$) was used to evaluate the heat-dissipation efficiency of TECs. The BN33 sample exhibited 42.5% higher $K_{\mathrm{Device}}^{\mathrm{eff}}$ than Bare at ΔT = 100 K. Moreover, IR imaging revealed that the filler can decrease the maximum temperature and ∇T in the TE legs. We envision that the proposed F-TEC concept can assist the development of an effective TEC device that can be widely used for hotspot cooling applications, such as in microprocessors, fuel cells, photovoltaic cells and batteries.

Although the cooling performance of the F-TECs was evaluated under heat load of 5.6 W/cm^2, smaller than that of practical hotspot cooling applications (e.g., 100 W/cm^2 for microprocessor), we expect further improvements by optimizing material properties and structural designs. Accordingly, we present considerations to improve the proposed F-TEC according to the following aspects. First, using high-κ filler materials can largely improve the cooling efficiency of an F-TEC for hotspot cooling, although we employed polymer–ceramic composites with relatively low κ in this study to exclude other technological challenges, such as matching the thermal expansion coefficients and suppressing electrical interferences between the TE legs and filler material. As the heat dissipation in an F-TEC is primarily unidirectional from the heat-loaded side to the heat sink (i.e. longitudinal), thermally anisotropic materials, such as transition metal dichalcogenides [51,52], hexagonal BN [53], and graphene [54], may be useful. Furthermore, the fillers are not limited to solid materials; highly thermally conductive liquid metals [55,56] could be considered fillers if outer surfaces of legs and bridges were electrically insulated by application of suitable layers. Second, the thermal expansion coefficient of the filler should be matched with those of the TE materials to reduce the thermomechanical stress in the TE legs [13,16,57], although this did not cause a significant problem in this study when using an elastic polymer composite filler. Third, the fill factor can be used as a design parameter to control the fractions of the Peltier and Fourier heat transfer, which mainly dissipate heat through the TE legs and filler, respectively. Fourth, although an F-TEC possess better cooling performance than a classical TEC, it requires more material and thus leads to increase in the device cost. Analyzing the thermoelectric operating cost (in units of $/kWh$_{th}$) may help to optimize the trade-off relation between the cooling performance and device cost [58]. Lastly, introducing thermal diodes may facilitate the development of a universal TEC that could be applicable for hotspot cooling, refrigeration, and under intermediate conditions. In addition to filler engineering, we emphasize the development of TE hotspot cooling materials with high κ and large PF [18–21,59]. By incorporating such materials and the F-TEC concept proposed in this study, the simultaneous optimization of PF and K_{Device}, and accordingly further performance improvement are expected.

CRediT authorship contribution statement

Sang J. Park: Conceptualization, Data curation, Formal analysis, Investigation, Methodology, Software, Validation, Visualization, Writing - Original Draft, Writing - Review & Editing. **Junyoung Park**: Data curation, Formal analysis, Investigation, Methodology, Validation, Writing - Review & Editing. **Ki Mun Bang**: Investigation, Methodology, Validation, Visualization, Writing - Review & Editing. **Jung Min Lee**: Data curation, Visualization. **Woosung Park**: Resources, Writing - Review & Editing. **Pawel Ziolkowski**: Validation, Writing - Review & Editing. **Hyungyu Jin:** Funding acquisition, Project administration, Resources, Supervision, Writing - Review & Editing.

Declaration of competing interest

The authors declare no competing financial interest.

Acknowledgments

This work was supported by Samsung Research Funding & Incubation Center of Samsung Electronics under Project Number SRFC-MA2002-02. This work was supported by National Research Foundation of Korea (NRF) grants funded by the Korea government (MSIT) (NRF-2020R1C1C1004291 and NRF-2022M3C1A3091988) and by the Ministry of Education, Science and Technology (NRF-2020K1A4A7A02095438) and by Basic Science Research Institute Fund (2021R1A6A1A10042944).

Appendix A. Supplementary Information

Supplementary Information associated with this article can be found, in the online version, at [DOI].

References

[1] Moore AL, Shi L. Emerging challenges and materials for thermal management of electronics. Mater Today 2014;17:163–74. https://doi.org/10.1016/j.mattod.2014.04.003.

[2] Wu W, Wang S, Wu W, Chen K, Hong S, Lai Y. A critical review of battery thermal performance and liquid based battery thermal management. Energy Convers Manag 2019;182:262–81. https://doi.org/10.1016/j.enconman.2018.12.051.

[3] Tang J, Ni H, Peng RL, Wang N, Zuo L. A review on energy conversion using hybrid photovoltaic and thermoelectric systems. J Power Sources 2023;562:232785. https://doi.org/10.1016/j.jpowsour.2023.232785.

[4] Bar-Cohen A, Wang P. Thermal management of on-chip hot spot. J Heat Transfer 2012;134:051017. https://doi.org/10.1115/1.4005708.

[5] Chowdhury I, Prasher R, Lofgreen K, Chrysler G, Narasimhan S, Mahajan R, et al. On-chip cooling by superlattice-based thin-film thermoelectrics. Nat Nanotechnol 2009;4:235–8. https://doi.org/10.1038/nnano.2008.417.

[6] Koester D, Venkatasubramanian R, Conner B, Snyder GJ. Embedded thermoelectric coolers for semiconductor hot spot cooling. Therm. Thermomechanical Proc. 10th Intersoc. Conf. Phenom. Electron. Syst. 2006. ITHERM 2006., IEEE; 2006, p. 491–6. https://doi.org/10.1109/ITHERM.2006.1645384.

[7] Ma M, Yu J, Chen J. An investigation on thermoelectric coolers operated with continuous current pulses. Energy Convers Manag 2015;98:275–81. https://doi.org/10.1016/j.enconman.2015.03.105.

[8] Snyder GJ, Soto M, Alley R, Koester D, Conner B. Hot spot cooling using embedded thermoelectric coolers. Twenty-Second Annu IEEE Semicond Therm Meas Manag Symp 2006:135–43.

[9] Solbrekken GL. Peltier enhanced heat spreading for localized hot spot thermal management. Proc ASME 2005 Pacific Rim Tech Conf Exhib Integr Packag MEMS, NEMS, Electron Syst Collocated with ASME 2005 Heat Transf Summer Conf Adv

Electron Packag Parts A, B, An 2005:2199–205. https://doi.org/10.1115/ipack2005-73471.

[10] Bell LE. Cooling, Heating, Generating Power, and Recovering Waste Heat with Thermoelectric Systems. Science (80-) 2008;321:1457–62.

[11] Zhao D, Tan G. A review of thermoelectric cooling: Materials, modeling and applications. Appl Therm Eng 2014;66:15–24. https://doi.org/10.1016/j.applthermaleng.2014.01.074.

[12] Ziabari A, Zebarjadi M, Vashaee D, Shakouri A. Nanoscale solid-state cooling: A review. Reports Prog Phys 2016;79:095901. https://doi.org/10.1088/0034-4885/79/9/095901.

[13] Zhang Q, Deng K, Wilkens L, Reith H, Nielsch K. Micro-thermoelectric devices. Nat Electron 2022;5:333–47. https://doi.org/10.1038/s41928-022-00776-0.

[14] Wang N, Zhang JN, Liu ZY, Ding C, Sui GR, Jia HZ, et al. An Enhanced Thermoelectric Collaborative Cooling System with Thermoelectric Generator Serving as a Supplementary Power Source. IEEE Trans Electron Devices 2021;68:1847–54. https://doi.org/10.1109/TED.2021.3059183.

[15] Sullivan O, Gupta MP, Mukhopadhyay S, Kumar S. Array of thermoelectric coolers for on-chip thermal management. J Electron Packag Trans ASME 2012;134:021005. https://doi.org/10.1115/1.4006141.

[16] Rowe DM. Thermoelectrics Handbook: Macro to Nano. 2006.

[17] Mao J, Chen G, Ren Z. Thermoelectric cooling materials. Nat Mater 2021;20:454–61. https://doi.org/10.1038/s41563-020-00852-w.

[18] Zebarjadi M. Electronic cooling using thermoelectric devices. Appl Phys Lett 2015;106:203506. https://doi.org/10.1063/1.4921457.

[19] Adams MJ, Verosky M, Zebarjadi M, Heremans JP. Active Peltier Coolers Based on Correlated and Magnon-Drag Metals. Phys Rev Appl 2019;11:054008. https://doi.org/10.1103/PhysRevApplied.11.054008.

[20] Li S, Snyder K, Akhanda S, Martukanitz R, Mitra M, Poon J, et al. Cost-efficient copper-nickel alloy for active cooling applications. Int J Heat Mass Transf 2022;195:123181. https://doi.org/10.1016/j.ijheatmasstransfer.2022.123181.

[21] Nimmagadda LA, Sinha S. Thermoelectric Property Requirements for On-Chip Cooling of Device Transients. IEEE Trans Electron Devices 2020;67:3716–21. https://doi.org/10.1109/TED.2020.3009085.

[22] Snyder GJ, Toberer ES. Complex TE meterials. Nat Mater 2008;7:105–14.

[23] Zhao LD, Lo SH, Zhang Y, Sun H, Tan G, Uher C, et al. Ultralow thermal conductivity and high thermoelectric figure of merit in SnSe crystals. Nature 2014;508:373–7. https://doi.org/10.1038/nature13184.

[24] He H, Fu R, Han Y, Shen Y, Song X. Thermal conductivity of ceramic particle filled polymer composites and theoretical predictions. J Mater Sci 2007;42:6749–54. https://doi.org/10.1007/s10853-006-1480-y.

[25] Joy J, George E, Haritha P, Thomas S, Anas S. An overview of boron nitride based polymer nanocomposites. J Polym Sci 2020;58:3115–41. https://doi.org/10.1002/pol.20200507.

[26] Li R, Yang X, Li J, Shen Y, Zhang L, Lu R, et al. Review on polymer composites with high thermal conductivity and low dielectric properties for electronic packaging. Mater Today Phys 2022;22:100594. https://doi.org/10.1016/j.mtphys.2021.100594.

[27] He X, Wang Y. Recent advances in the rational design of thermal conductive polymer composites. Ind Eng Chem Res 2021;60:1137–54. https://doi.org/10.1021/acs.iecr.0c05509.

[28] Hanemann T. Influence of particle properties on the viscosity of polymer-alumina composites. Ceram Int 2008;34:2099–105. https://doi.org/10.1016/j.ceramint.2007.08.007.

[29] Devaraj H, Giffney T, Petit A, Assadian M, Aw K. The development of highly flexible stretch sensors for a Robotic Hand. Robotics 2018;7:54. https://doi.org/10.3390/robotics7030054.

[30] Vaicekauskaite J, Mazurek P, Vudayagiri S, Skov AL. Mapping the mechanical and electrical properties of commercial silicone elastomer formulations for stretchable transducers. J Mater Chem C 2020;8:1273–9. https://doi.org/10.1039/c9tc05072h.

[31] 3M Boron Nitride Cooling Filler Platelets 2006;2006.

[32] Vu D, Zhang W, Şahin C, Flatté ME, Trivedi N, Heremans JP. Thermal chiral anomaly in the magnetic-field-induced ideal Weyl phase of Bi1−xSbx. Nat Mater 2021;20:1525–1531. https://doi.org/10.1038/s41563-021-00983-8.

[33] Frank P. Incropera, David P. DeWitt, Theodore L. Bergman ASL. Incropera's Principles of Heat and Mass Transfer. Willey; 2017.

[34] Wei J, Zhou W, Zhou W, Li S, Shen P, Ren S, et al. Modified Embedded Atom Method Potential for Modeling the Thermodynamic Properties of High Thermal Conductivity Beryllium Oxide. ACS Omega 2019;4:6339–46. https://doi.org/10.1021/acsomega.9b00174.

[35] Yazawa K, Shakouri A. Cost-efficiency trade-off and the design of thermoelectric power generators. Environ Sci Technol 2011;45:7548–53. https://doi.org/10.1021/es2005418.

[36] Witting IT, Chasapis TC, Ricci F, Peters M, Heinz NA, Hautier G, et al. The Thermoelectric Properties of Bismuth Telluride. Adv Electron Mater 2019;5:1800904. https://doi.org/10.1002/aelm.201800904.

[37] Bao D, Chen J, Yu Y, Liu W, Huang L, Han G, et al. Texture-dependent thermoelectric properties of nano-structured Bi2Te3. Chem Eng J 2020;388:124295. https://doi.org/10.1016/j.cej.2020.124295.

[38] Goncalves LM, Couto C, Alpuim P, Rolo AG, Völklein F, Correia JH. Optimization of thermoelectric properties on Bi2Te3 thin films deposited by thermal co-evaporation. Thin Solid Films 2010;518:2816–21. https://doi.org/10.1016/j.tsf.2009.08.038.

[39] SCHRODER DK. MATERIAL AND DEVICE SEMICONDUCTOR MATERIAL AND DEVICE Third Edition. Wiley; 2006.

[40] Suslov A V. Stand alone experimental setup for dc transport measurements. Rev Sci

Instrum 2010;81:075111. https://doi.org/10.1063/1.3463691.

[41] Lyu Y, Siddique ARM, Majid SH, Biglarbegian M, Gadsden SA, Mahmud S. Electric vehicle battery thermal management system with thermoelectric cooling. Energy Reports 2019;5:822–7. https://doi.org/10.1016/j.egyr.2019.06.016.

[42] Wehmeyer G, Yabuki T, Monachon C, Wu J, Dames C. Thermal diodes, regulators, and switches: Physical mechanisms and potential applications. Appl Phys Rev 2017;4:041304. https://doi.org/10.1063/1.5001072.

[43] Swoboda T, Klinar K, Yalamarthy AS, Kitanovski A, Muñoz Rojo M. Solid-State Thermal Control Devices. Adv Electron Mater 2021;7:2000625. https://doi.org/10.1002/aelm.202000625.

[44] Wong MY, Tso CY, Ho TC, Lee HH. A review of state of the art thermal diodes and their potential applications. Int J Heat Mass Transf 2021;164:120607. https://doi.org/10.1016/j.ijheatmasstransfer.2020.120607.

[45] Jin H, Restrepo OD, Antolin N, Boona SR, Windl W, Myers RC, et al. Phonon-induced diamagnetic force and its effect on the lattice thermal conductivity. Nat Mater 2015;14:601–6. https://doi.org/10.1038/nmat4247.

[46] Lu Q, Huberman S, Zhang H, Song Q, Wang J, Vardar G, et al. Bi-directional tuning of thermal transport in SrCoOx with electrochemically induced phase transitions. Nat Mater 2020;19:655–62. https://doi.org/10.1038/s41563-020-0612-0.

[47] Foley BM, Wallace M, Gaskins JT, Paisley EA, Johnson-Wilke RL, Kim JW, et al. Voltage-Controlled Bistable Thermal Conductivity in Suspended Ferroelectric Thin-Film Membranes. ACS Appl Mater Interfaces 2018;10:25493–501. https://doi.org/10.1021/acsami.8b04169.

[48] Lee S, Hippalgaonkar K, Yang F, Hong J, Ko C, Suh J, et al. Anomalously low electronic thermal conductivity in metallic vanadium dioxide. Science (80-) 2017;355:371–4. https://doi.org/10.1126/science.aag0410.

[49] Park SJ, Bang KM, Kim B, Ziolkowski P, Jeong J, Jin H. Adaptive thermoelectric cooling system for Energy-Efficient local and transient heat management. Appl Therm

Eng 2022;216:119060. https://doi.org/10.1016/j.applthermaleng.2022.119060.

[50] Barako MT, Park W, Marconnet AM, Asheghi M, Goodson KE. Thermal cycling, mechanical degradation, and the effective figure of merit of a thermoelectric module. J Electron Mater 2013;42:372–81. https://doi.org/10.1007/s11664-012-2366-1.

[51] Jiang P, Qian X, Gu X, Yang R. Probing Anisotropic Thermal Conductivity of Transition Metal Dichalcogenides MX2 (M = Mo, W and X = S, Se) using Time-Domain Thermoreflectance. Adv Mater 2017;29:1701068. https://doi.org/10.1002/adma.201701068.

[52] Kim SE, Mujid F, Rai A, Eriksson F, Suh J, Poddar P, et al. Extremely anisotropic van der Waals thermal conductors. Nature 2021;597:660–5. https://doi.org/10.1038/s41586-021-03867-8.

[53] Cai Q, Scullion D, Gan W, Falin A, Zhang S, Watanabe K, et al. High thermal conductivity of high-quality monolayer boron nitride and its thermal expansion. Sci Adv 2019;5:eaav0129. https://doi.org/10.1126/sciadv.aav0129.

[54] Balandin AA, Ghosh S, Bao W, Calizo I, Teweldebrhan D, Miao F, et al. Superior thermal conductivity of single-layer graphene. Nano Lett 2008;8:902–7. https://doi.org/10.1021/nl0731872.

[55] Kong W, Wang Z, Casey N, Korah MM, Uppal A, Green MD, et al. High Thermal Conductivity in Multiphase Liquid Metal and Silicon Carbide Soft Composites. Adv Mater Interfaces 2021;8:2100069. https://doi.org/10.1002/admi.202100069.

[56] Wang X, Lu C, Rao W. Liquid metal-based thermal interface materials with a high thermal conductivity for electronic cooling and bioheat-transfer applications. Appl Therm Eng 2021;192:116937. https://doi.org/10.1016/j.applthermaleng.2021.116937.

[57] He R, Schierning G, Nielsch K. Thermoelectric Devices: A Review of Devices, Architectures, and Contact Optimization. Adv Mater Technol 2018;3:1700256. https://doi.org/10.1002/admt.201700256.

[58] Leblanc S, Yee SK, Scullin ML, Dames C, Goodson KE. Material and manufacturing cost considerations for thermoelectrics. Renew Sustain Energy Rev 2014;32:313–27.

https://doi.org/10.1016/j.rser.2013.12.030.

[59] Luo H, Li X, Wang Y, Jin Y, Yao M, Yang J. High-throughput screening of room temperature active Peltier cooling materials in Heusler compounds. Npj Comput Mater 2022;8:199. https://doi.org/10.1038/s41524-022-00887-4.